

Article

Enhancing the Photovoltaic Properties via Incorporation of Selenophene Units in Organic Chromophores with $A_2-\pi_2-A_1-\pi_1-A_2$ Configuration: A DFT-Based Exploration

Muhammad Nadeem Arshad ^{1,2,*}, Iqra Shafiq ^{3,4}, Muhammad Khalid ^{3,4,*} , Mohammad Asad ^{1,2}, Abdullah M. Asiri ^{1,2} , Maha M. Alotaibi ², Atualpa A. C. Braga ⁵ , Anish Khan ^{1,2}  and Khalid A. Alamry ²

¹ Center of Excellence for Advanced Material Research (CEAMR), King Abdulaziz University, P.O. Box 80203, Jeddah 21589, Saudi Arabia

² Chemistry Department, Faculty of Science, King Abdulaziz University, P.O. Box 80203, Jeddah 21589, Saudi Arabia

³ Institute of Chemistry, Khwaja Fareed University of Engineering & Information Technology, Rahim Yar Khan 64200, Pakistan

⁴ Centre for Theoretical and Computational Research, Khwaja Fareed University of Engineering & Information Technology, Rahim Yar Khan 64200, Pakistan

⁵ Departamento de Química Fundamental, Instituto de Química, Universidade de Sao Paulo, Av. Prof. Lineu Prestes, 748, Sao Paulo 05508-000, Brazil; atualpa@iq.usp.br

* Correspondence: mnarshad@kau.edu.sa (M.N.A.); khalid@iq.usp.br (M.K.)

Abstract: Currently, polymer organic solar cells (POSCs) are widely utilized due to their significant application, such as low-cost power conversion efficiencies (PCEs). Therefore, we designed a series of photovoltaic materials (**D1**, **D2**, **D3**, **D5** and **D7**) by the incorporation of selenophene units ($n = 1-7$) as π_1 -spacers by considering the importance of POSCs. Density functional theory (DFT) calculations were accomplished at MPW1PW91/6-311G (d, p) functional to explore the impact of additional selenophene units on the photovoltaic behavior of the above-mentioned compounds. A comparative analysis was conducted for designed compounds and reference compounds (**D1**). Reduction in energy gaps ($\Delta E = 2.399 - 2.064$ eV) with broader absorption wavelength ($\lambda_{\max} = 655.480 - 728.376$ nm) in chloroform along with larger charge transference rate was studied with the addition of selenophene units as compared to **D1**. A significantly higher exciton dissociation rate was studied as lower values of binding energy ($E_b = 0.508 - 0.362$ eV) were noted in derivatives than in the reference ($E_b = 0.526$ eV). Moreover, transition density matrix (TDM) and density of state (DOS) data also supported the efficient charge transition origination from HOMOs to LUMOs. Open circuit voltage (V_{oc}) was also calculated for all the aforesaid compounds to check the efficiency, and significant results were seen (1.633–1.549 V). All the analyses supported our compounds as efficient POSCs materials with significant efficacy. These compounds might encourage the experimental researchers to synthesize them due to proficient photovoltaic materials.

Keywords: polymer organic solar cells; selenophene units; photovoltaic properties; $A_2-\pi_2-A_1-\pi_1-A_2$ configuration; DFT; open-circuit voltage



Citation: Arshad, M.N.; Shafiq, I.; Khalid, M.; Asad, M.; Asiri, A.M.; Alotaibi, M.M.; Braga, A.A.C.; Khan, A.; Alamry, K.A. Enhancing the Photovoltaic Properties via Incorporation of Selenophene Units in Organic Chromophores with $A_2-\pi_2-A_1-\pi_1-A_2$ Configuration: A DFT-Based Exploration. *Polymers* **2023**, *15*, 1508. <https://doi.org/10.3390/polym15061508>

Academic Editor: Shiyong Liu

Received: 12 January 2023

Revised: 8 March 2023

Accepted: 15 March 2023

Published: 17 March 2023



Copyright: © 2023 by the authors. Licensee MDPI, Basel, Switzerland. This article is an open access article distributed under the terms and conditions of the Creative Commons Attribution (CC BY) license (<https://creativecommons.org/licenses/by/4.0/>).

1. Introduction

Usually, inorganic solar cell structures were prepared by gallium arsenide (GaAs) and silicon (Si). They have attained great consideration because of their stability and high energy conversion efficiencies moving towards their theoretical limits for their precise bandgaps. Silicon-based solar cells (Si-SCs) used since today have a high proficiency of about 46% [1,2]. However, with the passage of time, the utilization of silicon has been reduced to a remarkable extent due to its fixed composition, non-tunable energy levels, brittleness, high cost and a limited number of atoms and compact structure. Consequently, researchers are now trying to substitute the silicon-based materials. A number of advantages, such as an easy

processability, low weight, cheaper and adaptable energy levels, have been observed for organic solar cells [3–5]. Organic SCs are fabricated on the elementary structure of inorganic SCs by substituting n-type and p-type with donors and acceptors [6–8]. Dye-sensitized solar cells (DSSCs) were gaining considerable attention due to their significant photovoltaic performances. Moreover, DSSCs have low costs, great stability and tunable visual properties, such as transparency and color [9,10]. The dye in DSSCs catches special attention due to its ability to convert light into electricity by photoexcitation phenomena [11]. Further, DSSCs are reported with significant efficiency, facile synthetic route and purification. DSSCs have many tunable optical properties through easy modifications in chemical structures [12]. Moreover, the photovoltaic world is enriched with many interesting materials, such as organic solar cells' fullerene derivatives such as PC61BM, PC71BM and ICBA. The fullerene-based OSCs are found with the following remarkable properties: tunable energy levels, simple processability, lightweight, large area of fabrication and mechanical flexibility [3–5,13–15]. Owing to the following limitations: limited absorption behavior and larger molecular weight of fullerene [16] the main focus of researchers has been moved towards non-fullerene organic solar cells (NF-OSCs) as they obtained many significant findings in NF-OSCs [17–19]. Recently, NF-OSCs gained considerable attention from researchers due to their high flexibility, pellucid nature and tunable energy level [14,20,21]. The literature revealed many reports where organic systems with the following various architectures: donor-acceptor, donor- π -linker-acceptor- π -spacer-donor, donor- π spacer-acceptor, donor-donor- π -acceptor, acceptor- π -spacer-donor- π -linker-acceptor and donor-acceptor- π -acceptor. These architectures are widely utilized for significant OSCs materials [22,23]. Further, NFAs are blended with donor polymers and, subsequently, optical absorption properties are improved. These phenomena aided to enhance the PCE of single-junction cells by up to 17% [24]. Apart from this, there is also found some of the following features of non-fullerene acceptors (NFAs) derivatives: facile synthesis [13,21], material design [25,26] and realization of the mechanism and their optimization [27,28]. They have contained the approach for rationalizing significant PCEs over 18% [29]. In addition, stability tests of NFAs have been performed and data reveal that NFAs-based OSCs may obtain a life span of up to 10 years, which reveals their promising values for practical application [30,31]. The NF-OSCs are categorized into the following two groups: small molecular acceptor (SMA) and polymer organic solar cells (POSCs) [6,7,32]. Recently, the POSCs gained the attention of the researchers as efficient photovoltaic materials due to their improved open-circuit voltage (V_{oc}) and significantly low price PCEs [33–36]. In the current century, devotion is paid to engineering polymer bulk hetero-junction (BHJ) SCs initiated on fullerene donors and fullerene-free polymeric acceptors, progressing efficiency to 8.3% [37]. Conjugative POSCs attracted significant attention due to their efficient ability to absorb sunlight and tunable electronic characteristics and good PCEs [38,39]. The π -resonance and behavior of substituents control the band gap, influence the charge transfer and enhanced photovoltaic properties [22,40]. Different strategies and criteria are present in the literature, which imply fine-tuning of acceptor-donor blend to boost UV-Visible absorption, resulting in uplifted short circuit current density (J_{sc}), lessening of the energy gap between HOMO and LUMO, optimized morphology of blend to increase the fill factor (FF) and open-circuit voltage (V_{oc}).

Keeping in consideration the aforementioned aspects, here we have taken an NF-based synthesized parent compound, namely, 2,2'-((2E,2'E)-((6,6'-(2,5-difluoro-1,4-phenylene)bis(4,4-bis(2-ethylhexyl)-4H-cyclopenta [1,2-b:5,4-b']dithiophene-6,2-diyl))bis(methanylylidene))bis(3-oxo-2,3-dihydro-1H-indene-2,1-diylidene))dimalononitrile abbreviated as **DF-PCIC** [41] having A_2 - π_2 - A_1 - π_1 - A_2 configuration. After replacing 4,4-dimethyl-4H-cyclopenta [1,2-b:5,4-b']dithiophene with a selenophene ring as the first π -spacer (π_1) and via substituting both the terminal acceptors with benzothiophene acceptors (A_2) on both sides, the parent compound is modified into a reference compound, which is denoted as **D1**. From the literature, we found that selenophene units and benzothiophene acceptors can lower the LUMO level with an unchanged HOMO level and effectively improve the V_{oc} and J_{sc} in POSCs [42–45]. Therefore, in the current study, we performed molecular engineering of **D1**

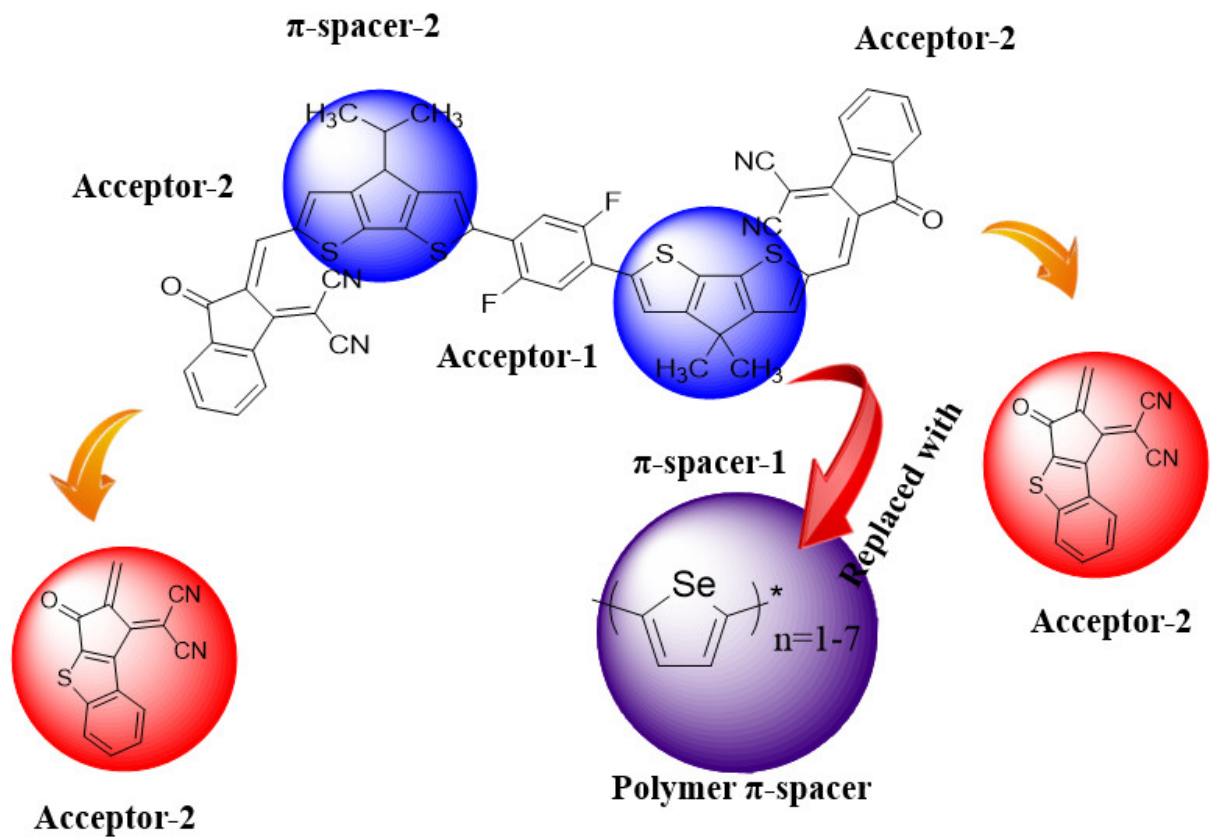
with a selenophene ring and benzothiophene acceptors to improve the V_{oc} . **D2**, **D3**, **D5** and **D7** compounds. These compounds were designed by the incorporation of selenophene units ($n = 2-7$) in this reference (**D1**). The influence of structural modifications on electronic and optical behavior is explored in this research paper through DFT. It is predicted that the designed derivatives might be beneficial for the engineering of highly efficient OSCs.

2. Computational Procedure

The Gaussian 09 program [46] was employed to perform the calculations of current research work. First of all, geometries of aforesaid chromophores were optimized at MPW1PW91 functional with 6-311 G (d, p) basis set to obtain geometries at true minima. With the aid of Gauss View 5.0 [47], the input files were drawn. To find the photovoltaic properties of selenophene derivatives (**D1**, **D2**, **D3**, **D5** and **D7**), various kinds of analyses such as DOS, V_{oc} , E_b , μ_{tot} and GRPs were accomplished at the aforesaid level of DFT by utilizing the optimized structures. Nevertheless, the following key electronic properties: TDM, FMO analysis and optical properties, were investigated through TD-TDF at the above-mentioned functional. To interpret the results from output files, multiple software such as; Avogadro [48], Gauss Sum [49], Chemcraft [50], Multiwfn 3.7 [51] and PyMOLyze 2.0 [52], Origin 8.5 program [53] were utilized.

3. Results and Discussion

Nowadays, polymer organic solar cells (POSCs) are widely utilized as photovoltaic devices due to their low-cost sunlight conversion efficiencies [54,55]. The literature is flooded with many reports in which small units, such as thiophene, selenophene and imidazole, etc. were utilized to improve the charge transference properties of organic systems [8,42,56]. From the literature, we found that by replacing the sulfur with a selenium atom, a significant reduction in band gap can be achieved [57]. The current approach aims to explore the effect of selenophene unit on charge transference rate between orbitals and also described the influence on the photovoltaic properties of organic systems. For this purpose, a synthesized fullerene-free organic system (**DF-PCIC**) is chosen as a parent molecule to design reference compounds (**D1**) with an $A_2-\pi_2-A_1-\pi_1-A_2$ framework. First of all, the π -bridge (4H-cyclopenta [1,2-b:5,4-b']dithiophene) on the one side of **DF-PCIC** is replaced with selenophene and kept the other side preserved. The terminal acceptors (2-(2-methylene-3-oxo-2,3-dihydro-1H-inden-1-ylidene)malononitrile) in **DF-PCIC** are replaced with a benzothiophene-based acceptor (2-(2-methylene-3-oxo-2,3-dihydro-1H-benzo[b]cyclopenta[d]thiophen-1-ylidene)malononitrile) in order to improve the electron-withdrawing effect in **D1** (Scheme 1 and Figure 1). Then **D1** is considered a reference molecule, and further, it is utilized to design other derivatives (**D2**, **D3**, **D5** and **D7**). The **D2** and **D3** are designed by introducing two and three units of selenophene, respectively, keeping the same acceptors as shown in Figure 1. Furthermore, to explore the effect of the high number of selenophene units on the photovoltaic responses of POSCs, we introduce five and seven units of selenophene, respectively, in **D5** and **D7** (Figure 1). The IUPAC names of reference (**D1**) and their derivatives (**D2**, **D3**, **D5** and **D7**) are explained in the Supplementary File. The true minima structures of the above-mentioned POSCs are displayed in Figure 2, and their cartesian coordinates are tabulated in Tables S1–S5.



Scheme 1. The sketch map of designed chromophores (D1, D2, D3, D5 and D7). From parent molecule (DF-PCIC).

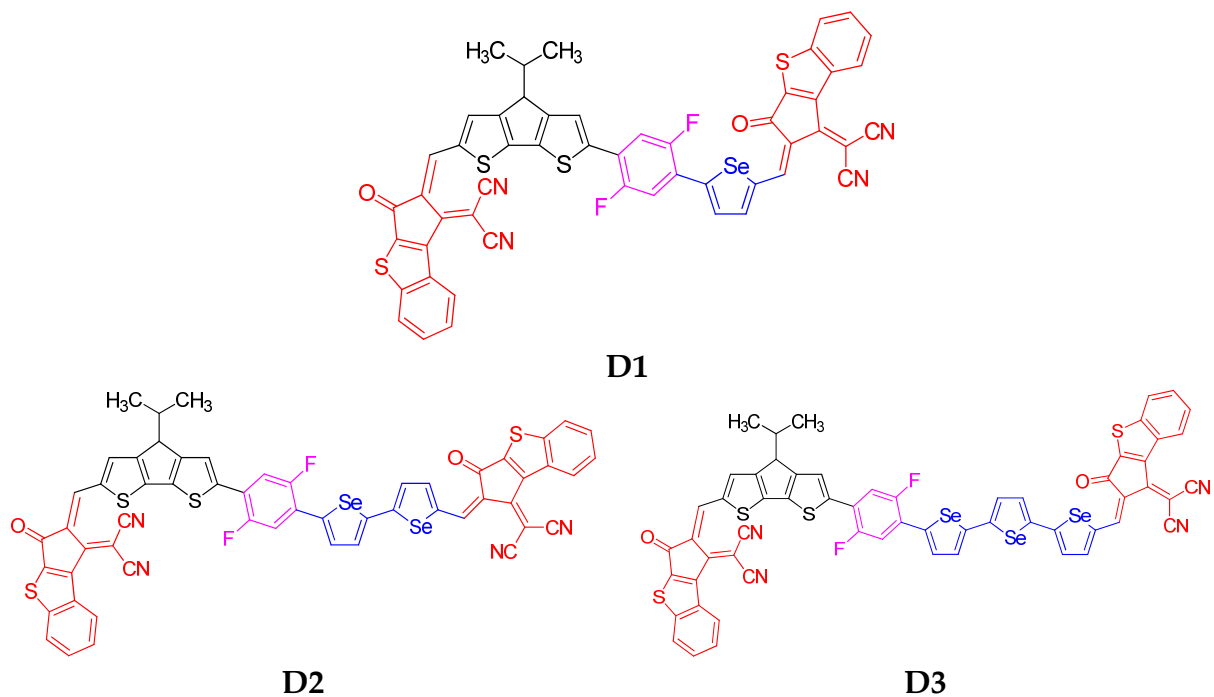


Figure 1. Cont.

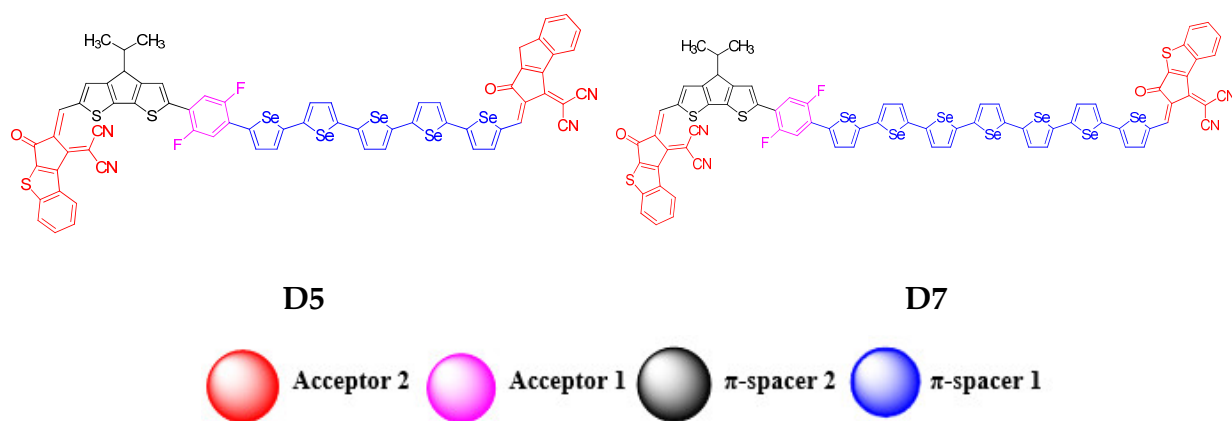


Figure 1. The 2D geometries of D1, D2, D3, D5 and D7.

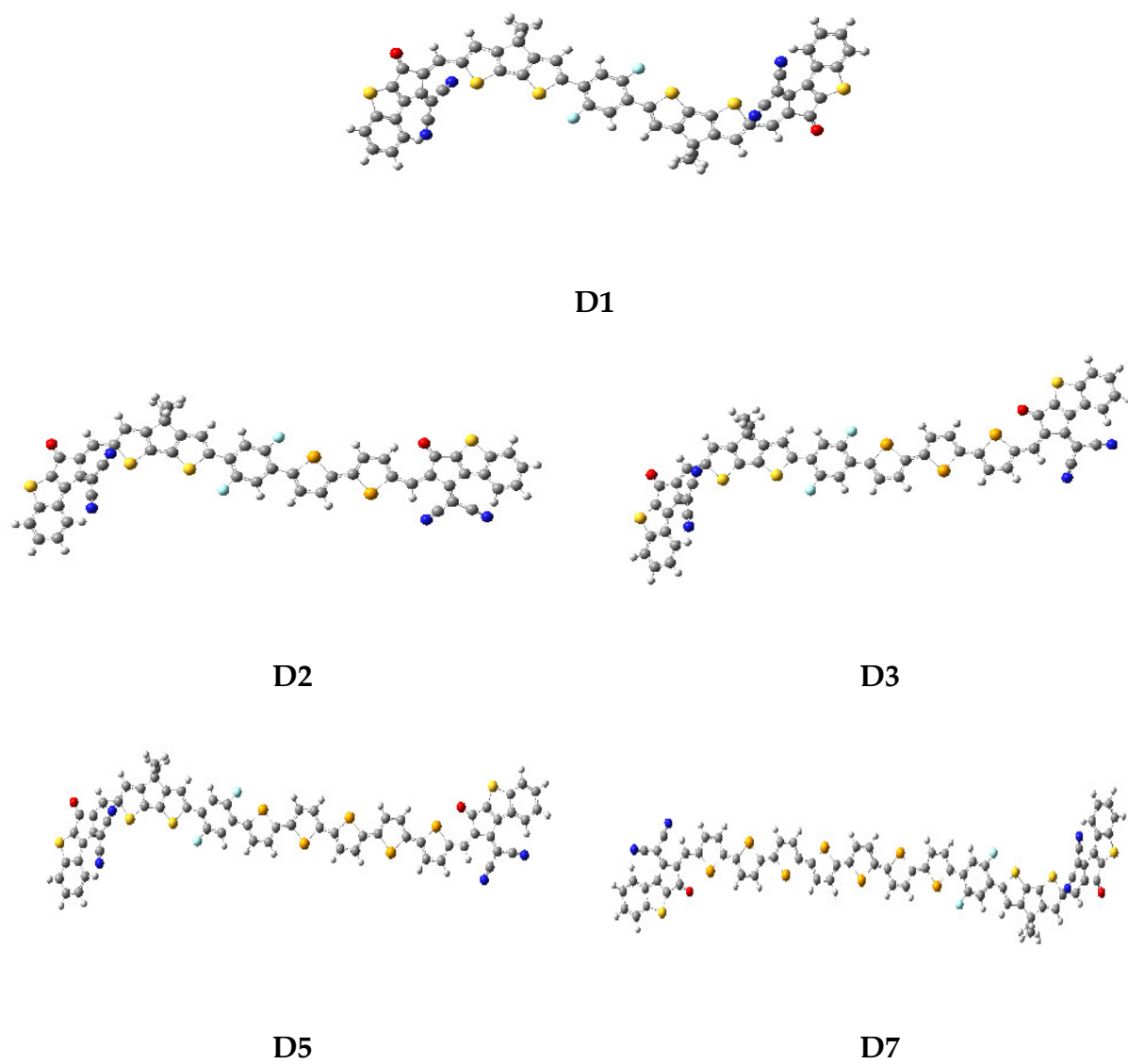


Figure 2. True minima structures of selenophene-based derivatives.

4. Frontier Molecular Orbital (FMO) Analysis

FMO analysis is deliberated as a leading method to estimate the electronic properties of organic systems [58,59]. FMOs are indispensable to accelerating the transmission of electric current and provide the properties of photovoltaic cells with the aptitude for conducting electronic charges [60,61]. In accordance with the valence band theory, HOMO is considered a valence band, while LUMO is regarded as a conduction band. The band gap of HOMO and LUMO is a substantial factor in elucidating several quantum chemical parameters such as chemical reactivity, charge transfer, UV-Visible spectrum, chemical stability and electronic properties [62–64]. The potent photovoltaic response is indicated by less energy difference that reasonably determines the efficiency of a compound [65]. The calculated HOMO-LUMO energies as well as their energy gaps for designed molecules, are composed in Table 1.

Table 1. E_{LUMO} , E_{HOMO} and energy gaps ($E_{gap} = E_{LUMO} - E_{HOMO}$) of **D1**, **D2**, **D3**, **D5** and **D7**.

Chromophores	E_{HOMO}	E_{LUMO}	E_{gap}
D1	−5.845	−3.380	2.465
D2	−5.744	−3.345	2.399
D3	−5.636	−3.329	2.307
D5	−5.472	−3.305	2.167
D7	−5.361	−3.297	2.064

Units in eV.

Table 1 illustrates that the energies of HOMO/LUMO for **D1** are established to be −5.845/−3.380 eV with a 2.465 eV energy gap. While the HOMO/LUMO energies for its derivatives (**D2**, **D3**, **D5** and **D7**) are recorded as −5.744/−3.345, −5.636/−3.329, −5.472/−3.305 and −5.361/−3.297 eV and their energy gaps are computed as 2.399, 2.307, 2.167 and 2.064 eV, respectively. The declining E_{gap} noticed from **D1** to **D7** might be due to the continual addition of selenophene monomer in π_1 in each designed compound extending the conjugation and boosting the charge transfer. The charge transfer of a chromophore is indirectly related to the E_{gap} , i.e., the lower the E_{gap} , the greater the charge transfer and vice versa [66,67]. The overall declining trend of E_{gap} is viewed as **D1** (2.465 eV) > **D2** (2.399 eV) > **D3** (2.307 eV) > **D5** (2.167 eV) > **D7** (2.064 eV). The effective charge mobility from acceptor−2 to acceptor−1 through π -spacer along with the lowest E_{gap} among the molecular orbitals are noticed in **D7** chromophore than other designed molecules, which emerged to be an efficient material for use in photovoltaic devices.

The FMOs contour surface diagrams are illustrated in Figure 3, which expresses the distribution of electronic clouds over the molecules. In **D1** and **D2**, charge density is significantly concentrated on the central part, while a little bit of electronic density is noticed on terminal acceptor entities in HOMO and LUMO. In **D3**, **D5** and **D7**, HOMO is majorly concentrated on the acceptor−2 and π -bridge, whereas LUMO is mainly located in electron-deficient end-capped groups. Hence, the analyzed molecular systems showed charge transmission from acceptor−2 to acceptor−1 through the π -bridge. The energies of HOMO-1/LUMO+1 and HOMO-2/LUMO+2 are illustrated in Table S6, while their FMO diagrams are displayed in Figures S1–S5. Almost the same phenomena for energies and charge transference are seen between higher orbitals (HOMO-1/LUMO+1 and HOMO-2/LUMO+2).

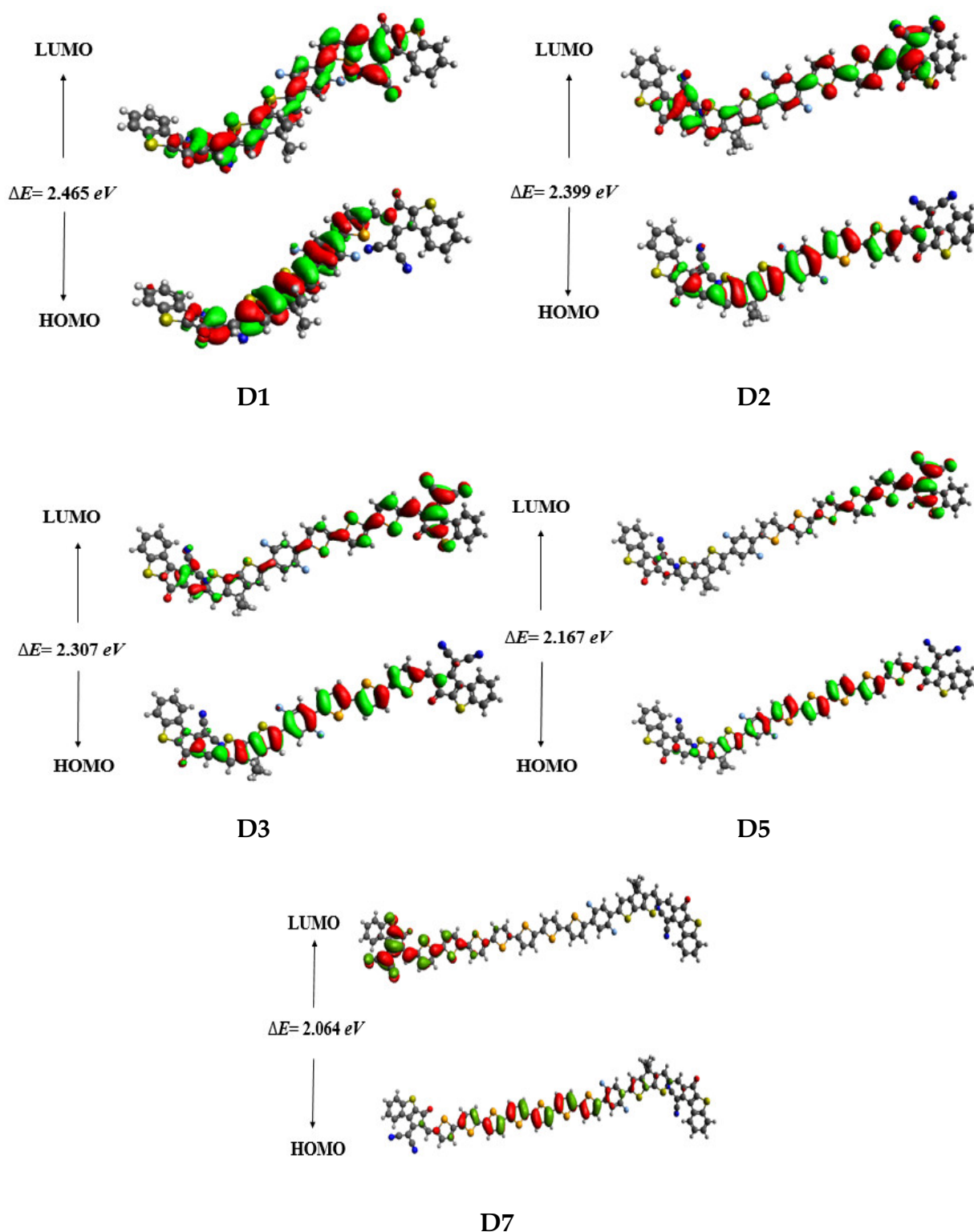


Figure 3. FMO diagrams of studied compounds.

5. Optical Properties

A UV-Visible analysis is a significant tool to elucidate the probability of charge transference, the nature of electronic transitions and contributing configuration in transitions within the chromophores [68,69]. TD-DFT calculations were performed at MPW1PW91/6-311 G (d,p) level in chloroform and gaseous phase to assess the photophysical properties of the designed chromophores. The main outcomes of oscillator strength (f_{os}), transition

energy (E) and maximum absorption wavelengths (λ_{max}) are collected in Tables 2 and 3 in gas and chloroform, respectively, and their graphs are presented in Figure 4. Moreover, other results are exhibited in Tables S8–S17.

Table 2. The calculated transition energies (eV), maximum absorption wavelengths (λ_{max}), oscillator strengths (f_{os}) and transition natures of **D1**, **D2**, **D3**, **D5** and **D7** in gas phase.

Compounds	DFT λ (nm)	E (eV)	f_{os}	MO Contributions
D1	596.393	2.078	1.872	H→L (91%)
D2	613.722	2.020	2.750	H→L (90%)
D3	635.490	1.951	3.075	H→L (88%)
D5	668.702	1.854	3.524	H→L (84%)
D7	691.953	1.791	3.708	H→L (77%)

MO = molecular orbital, f_{os} = oscillator strength, H = HOMO, L = LUMO.

Table 3. Computed absorption properties of **D1**, **D2**, **D3**, **D5** and **D7** in chloroform solvent.

Compounds	DFT λ (nm)	E (eV)	f_{os}	MO Contributions
D1	639.390	1.939	1.879	H→L (86%)
D2	655.480	1.891	2.674	H→L (85%)
D3	676.474	1.832	3.0738	H→L (82%)
D5	708.521	1.749	3.395	H→L (80%)
D7	728.376	1.702	3.409	H→L (75%)

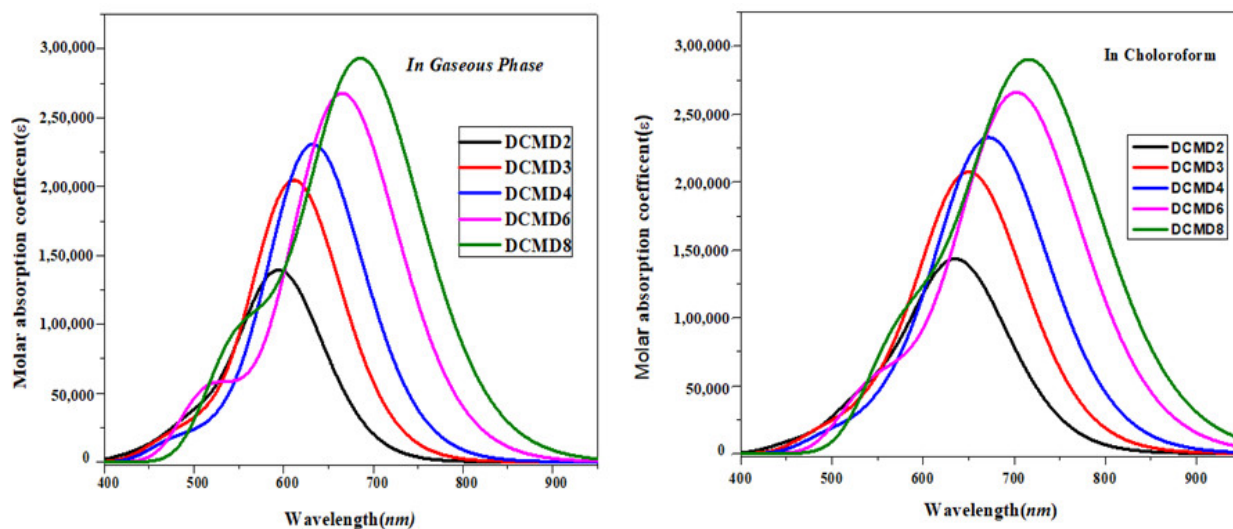


Figure 4. Absorption spectra of entitled compounds i.e.

Table 2 shows that the absorption values of **D1**, **D2**, **D3**, **D5** and **D7** in the range of 596.393–691.953 nm with 1.872–3.708 oscillation strength and 1.791–2.078 eV transition energy in the gas phase are found. The strongest absorption of 691.953 nm is exhibited by **D7**, which might be because of the extended conjugation and effective intramolecular charge transfer. The increasing λ_{max} order is found to be **D1** (596.393 nm) < **D2** (613.722 nm) < **D3** (635.490 nm) < **D5** (668.702 nm) < **D7** (691.953 nm).

In chloroform solvent, the λ_{max} values of titled molecules are obtained to be 639.390, 655.480, 676.474, 708.521 and 728.376 nm for **D1**, **D2**, **D3**, **D5** and **D7**, respectively (Table 3). The values of λ_{max} are observed as **D7** (728.376 nm) > **D5** (708.521 nm) > **D3** (676.474 nm) > **D2** (655.480 nm) > **D1** (639.390 nm). This enhancement might be regarded as the continuous addition of selenophene units in the first π -spacer (π_1) in each derivative, which results in extending the conjugation and boosting the charge transfer. Meanwhile, the absorption

wavelength of these molecules is compared in the solvent phase to that in the gaseous phase, and it is noticed that λ_{max} in chloroform is also examined to be greater than the gas phase due to the solvent effect. Overall, the maximum bathochromic shift is observed for **D7** in both phases, so these designed chromophores can be regarded as excellent solar cell material for future use.

5.1. Global Reactivity Parameters (GRPs) Investigations

To investigate the stability and reactivity of a molecule, GRPs are calculated through the energies of HOMOs and LUMOs. The global softness (σ), electron affinity (EA), global hardness (η), global electrophilicity index (ω), chemical potential (μ), ionization potential (IP) and electronegativity (X) were computed by using the band gap of HOMO and LUMO [70–74]. The following Equations (1) and (2) are used to calculate EA and IP .

$$IP = -E_{HOMO} \quad (1)$$

$$EA = -E_{LUMO} \quad (2)$$

Koopmans's theorem is utilized to determine σ , ω , η , μ and X [75].

$$X = \frac{[IP + EA]}{2} \quad (3)$$

$$\eta = \frac{[IP - EA]}{2} \quad (4)$$

$$\mu = \frac{E_{HOMO} + E_{LUMO}}{2} \quad (5)$$

$$\sigma = \frac{1}{2\eta} \quad (6)$$

$$\omega = \frac{\mu^2}{2\eta} \quad (7)$$

The above parameters were obtained utilizing Equations (1)–(7), and these results are displayed in Table 4. The chemical potential of a molecule expresses the stability and reactivity of a specie. IP signifies the electron donating and accepting ability, which is the energy requires to eradicate the electron from HOMO. The energy gap, chemical potential, stability and hardness are inversely associated with reactivity while directly to one another [69]. Moreover, the stability of a molecule depends upon the electronegativity and the position of its substituents with respect to the electronegative atom [76]. Thus, the molecule with greater energy difference is considered harder, which shows low reactivity and high kinetic stability.

Table 4. Global reactivity parameters of **D1**, **D2**, **D3**, **D5** and **D7**.

Compounds	IP	EA	X	η	μ	ω	σ
D1	5.845	3.380	4.613	1.233	−4.613	8.631	0.406
D2	5.744	3.345	4.545	1.199	−4.545	8.609	0.417
D3	5.636	3.329	4.483	1.154	−4.483	8.709	0.434
D5	5.472	3.305	4.389	1.084	−4.389	8.888	0.461
D7	5.631	3.297	4.464	1.167	−4.464	8.538	0.428

Units in eV.

The IP values are noted to be greater in magnitude than EA values. The hardness values are noticed as 1.233, 1.199, 1.154, 1.084 and 1.167 eV for **D1**, **D2**, **D3**, **D5** and **D7**, respectively, and its descending order is found in studied molecules as **D1** > **D2** > **D7** > **D3** > **D5**. The hardness of a molecule is directly linked with the E_{gap} and inversely related to the reactivity. Therefore, a chromophore with a greater energy gap is considered harder

and more stable [77]. Another factor that discloses the reactivity of molecules is softness, which is directly associated with polarizability [78]. The softness value calculated for **D5** is observed to be 0.461 eV, which reduces to 0.434 eV in **D3** and further declines to 0.428 eV for **D7**, while the least value (0.417 eV) is noted in **D2**. Interestingly, the highest value of softness (0.461 eV) is viewed in **D5**, which might be due to an increase in conjugation due to an extended π -spacer. Thus, it is regarded as the most polarizable and exhibits good photovoltaic properties for all the said chromophores.

5.2. The Density of State (DOS) Analysis

The DOS analysis is accomplished to estimate the contribution of each fragment of the molecule in the total electronic distribution and absorption band [42,79]. To perform this analysis, the designed molecules are partitioned into four fragments, i.e., acceptor-2, π -spacer-2, acceptor-1 and π -spacer-1. DOS was carried out for **D1**, **D2**, **D3**, **D5** and **D7** to support the insights obtained from FMO exploration [80]. The DOS pictographs are displayed in Figure 5, where each fragment is presented in different colors (acceptor-2 with red, acceptor-1 with green, π -spacer-2 with blue and π -spacer-1 with pink lines). The pattern of electronic charge dissemination is altered by changing acceptor moieties and extending the π -spacer, which is justified by the DOS percentage of HOMO-LUMO. Herein, acceptor-1 depicted 14.1, 14.7, 13.0, 7.2 and 4.2% charge distribution pattern to HOMO, whereas 9.8, 7.1, 3.8, 1.0 and 0.2% to LUMO for **D1**, **D2**, **D3**, **D5** and **D7**, respectively. Likewise, acceptor-2 showed charge contributions as follows: 22.4, 18.5, 14.1, 7.4 and 3.7% to HOMO, while 60.0, 53.4, 59.1, 61.8 and 64.0% to LUMO. Furthermore, π -spacer-1 demonstrates an electronic distribution pattern as follows: 8.7, 24.6, 45.3, 74.8 and 87.3% to HOMO, whereas 15.3, 26.9, 30.0, 35.1 and 35.5% to LUMO in **D1**, **D2**, **D3**, **D5** and **D7**, correspondingly. Similarly, π -bridge-2 manifested a pattern of electronic distribution as follows: 54.8, 42.2, 27.6, 10.6 and 4.8% to HOMO, while 60.0, 53.4, 59.1, 61.8 and 64.0% to LUMO, accordingly. It is clear from these outcomes that HOMO is predominantly located on acceptor-1, while LUMO mainly resides on acceptor-2 in the aforementioned compounds. Overall, the pattern of electronic charge distribution unveils that a significant amount of charge is shifted from HOMO to LUMO, exhibiting them as promising candidates for fullerene-free OSCs.

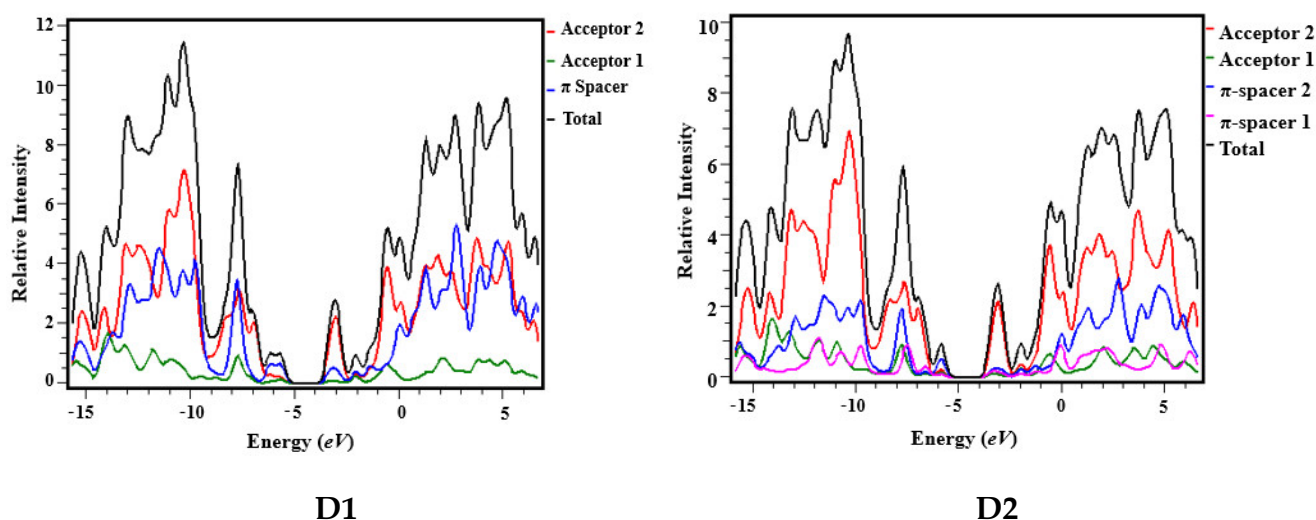


Figure 5. Cont.

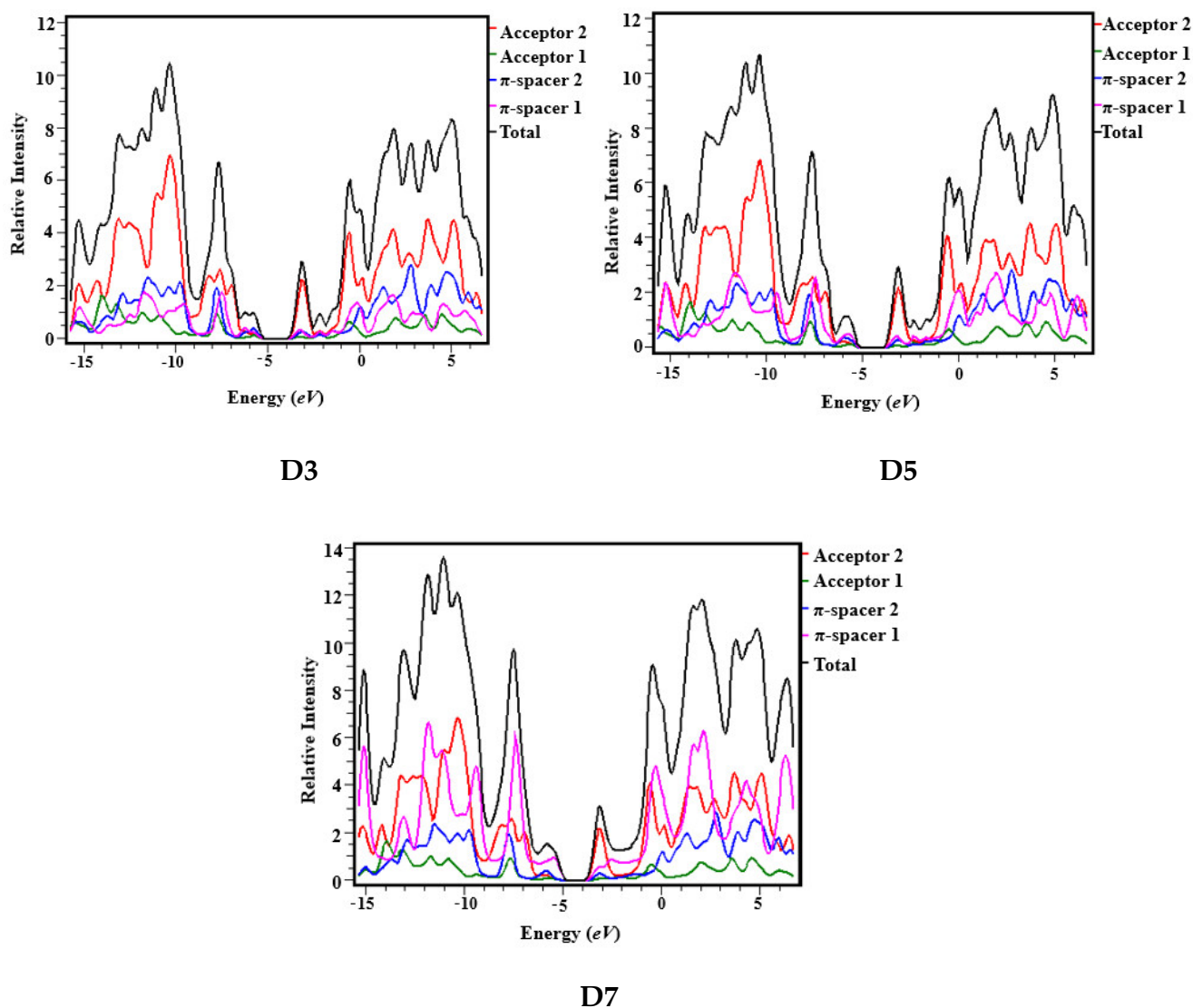


Figure 5. Graphical representation of DOS spectra for D1, D2, D3, D5 and D7.

5.3. Transition Density Matrix (TDM) Study

The interpretation of the transition process in a conjugated system can be effectively determined by utilizing TDM analysis [81,82]. The TDM investigation presents a three-dimensional heat map for transition among two eigenstates. It depicts the scattering of electrons as well as hole pairs and permits to analyze their coherence lengths and delocalization [83,84]. The pictorial representation of interaction among acceptor and donor entities in the S1 (excited) state is represented by the blue region in the spatial map [42,85]. The emission and absorption of studied molecules, i.e., D1, D2, D3, D5 and D7 were examined at TD-DFT/MPW1PW91 functional and 6–311 G (d,p) basis set. The effect of a hydrogen atom is ignored owing to its minor involvement in an electronic transition. The pictographs of TDM are displayed in Figure 6 with different fragments on the left side and bottom, whereas electron density is reported on the y-axis.

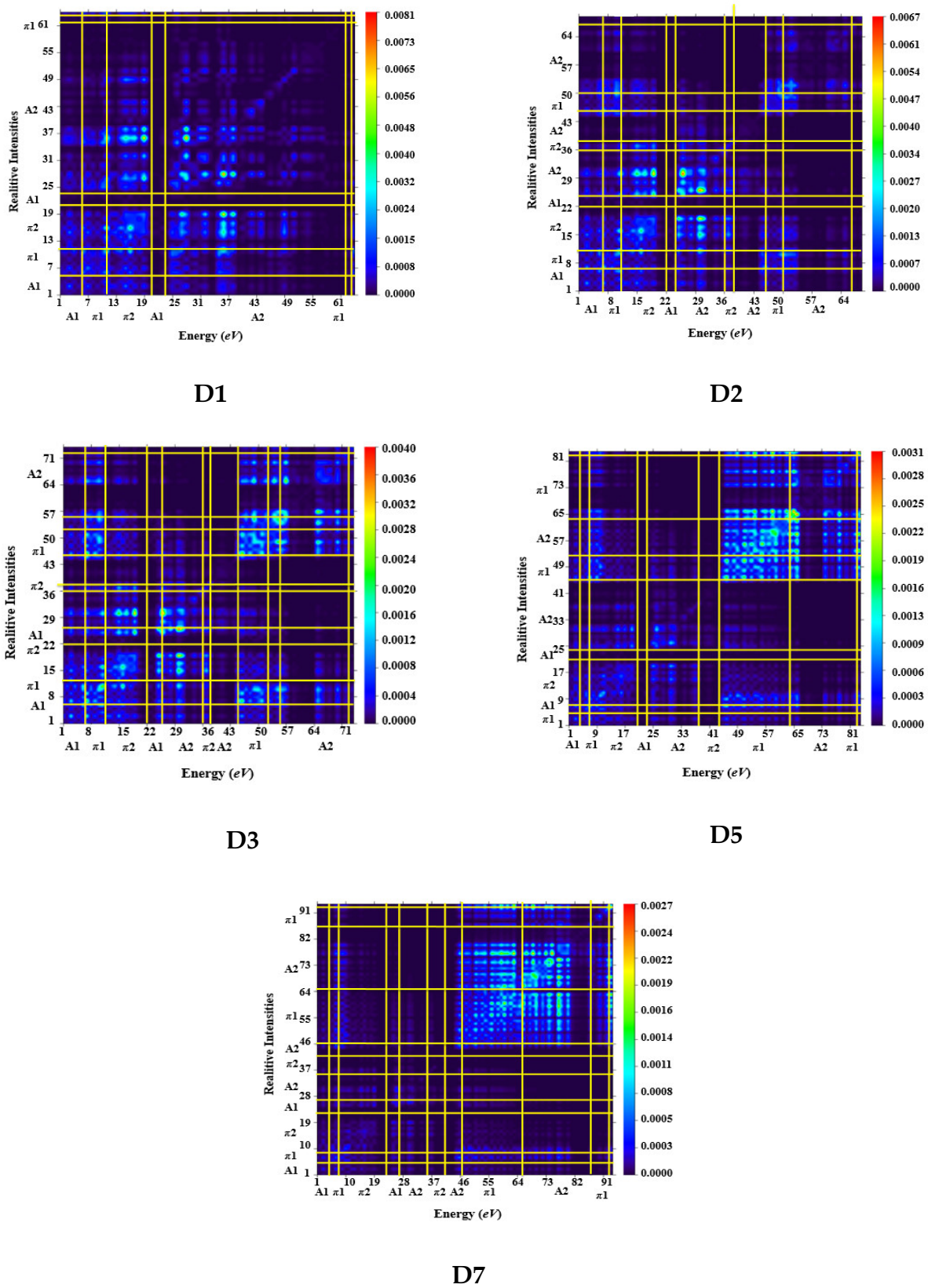


Figure 6. TDM graphs of the D1, D2, D3, D5 and D7 at the S1 states.

The uniform dissemination of electrons over the molecule diagonal transfer can be viewed from the bright portion of TDM graphs for all the computed molecules (D1, D2, D3, D5 and D7). Moreover, electron-hole pair generation and charge coherence also

appeared to proliferate non-diagonally. FMO findings revealed that the charge density is considered observed over the molecule, which causes notable variation in TDM plots. Figure 6 displayed that the electron density effectually transfers from the core to terminal acceptors through π -spacers in **D1**, **D2**, **D3**, **D5** and **D7** allowing efficient charge transfer.

Binding energy (E_b) is another significant factor to estimate the photovoltaic response of the examined molecules. A lesser E_b value results in a greater exciton dissociation in the S1 state due to less coulomb's force between the electron and hole. The E_b of **D1**, **D2**, **D3**, **D5** and **D7** are calculated from the energy of optimization (E_{opt}) and the HOMO-LUMO energy gap (E_{gap}) [86] as shown in Equation (8) and the computed outcomes are listed in Table 5.

$$E_b = E_{L-H} - E_{opt} \quad (8)$$

Table 5. Computed binding energies (E_b) of **D1**, **D2**, **D3**, **D5** and **D7**.

Chromophores	E_{H-L}	E_{opt}	E_b
D1	2.465	1.939	0.526
D2	2.399	1.891	0.508
D3	2.307	1.832	0.475
D5	2.167	1.749	0.418
D7	2.064	1.702	0.362

Units in eV.

According to the outcomes collected in Table 5, an almost similar trend to the FMOs energy gap is noticed in the first singlet exciton energy, i.e., it decreases gradually from **D1**, **D2**, **D3**, **D5** and **D7**. Moreover, the values of E_b for the titled compounds are obtained to be 0.526, 0.508, 0.475, 0.418 and 0.362 eV, respectively. The least value of E_b (0.362 eV) is investigated in **D7**, among all the designed chromophores, which illustrates that it has the highest capacity of exciton dissociation and enhanced current charge density (J_{sc}). The decreasing order of E_b is obtained as follows: **D1** > **D2** > **D3** > **D5** > **D7**. Interestingly, all the studied chromophores showed lower E_b values than that of **D1** and might be used for photovoltaic applications.

5.4. Dipole Moment (μ_{tot}) Analysis

The dipole moment (μ_{tot}) of a molecule is directly influenced by electronegativity (E.N) difference, the greater the E.N difference, the greater would be the dipole moment (μ_{tot}) [72]. The dipole moment values of **D1**, **D2**, **D3**, **D5** and **D7** in x, y and z directions are calculated and collected in Table 6.

Table 6. Computed dipole moment (μ_{tot}) of **D1**, **D2**, **D3**, **D5** and **D7**, μ units in D.

Chromophores	μ_x	μ_y	μ_z	μ_{total}
D1	0.7967	1.9193	−0.6419	2.1750
D2	3.8529	5.4304	5.1333	8.4074
D3	−1.5910	8.3120	−5.2673	9.9682
D5	−3.8684	−5.9795	1.6921	7.3200
D7	−1.7431	3.5215	−3.9342	5.5604

The data from the above table illustrate that **D3** depicted the largest value of μ_{tot} (9.9682 D) of all the entitled chromophores. Overall, the decreasing order of μ_{tot} is as follows: **D3** > **D2** > **D5** > **D7** > **D1**. The superior μ_{tot} values of the entitled compounds exploited the greater polarizability in them, which indicates the higher charge transference, resulting in effective photovoltaic responses.

5.5. The Open-Circuit Voltage (V_{oc}) Investigations

The open-circuit voltage (V_{oc}) is an interesting approach that plays an important role in determining the performance of the OSCs [87,88]. In fact, it explains the maximum current that may be achieved from an optical substance [89]. The following influential factors affecting the V_{oc} are found: light intensity, light source, external fluorescence proficiency, OSCs device's temperature, charge carrier recombination and various other environmental elements. The V_{oc} is closely related to the energy difference between HOMO and LUMO of the donor (D) and acceptor (A) compounds [90]. In order to attain a higher V_{oc} , in the acceptor molecule, the LUMO level should be lower and for the donor molecule, the HOMO level should be with a high energy level [91]. Equation (9) is used to calculate the V_{oc} for the designed materials, as provided by Scharber and his coworkers [92].

$$V_{oc} = \left(\left| E_{HOMO}^D \right| - \left| E_{LUMO}^A \right| \right) - 0.3 \quad (9)$$

Hence, E is an elementary charge of acceptors, signifies the charge on each molecule, and 0.3 denotes the empirical constant. The chlorinated polymer **J52-Cl** is a well-known donor polymer widely used in large published reports to blend with acceptor molecules in charge transfer analysis. [93–96]. Therefore, following the literature, the studied molecules are blended with **J52-Cl** polymer to predict the potential usage of designed compounds regarding charge transfer characteristics for organic solar cells. The structural representation of **J52-Cl** is shown in Figure 7. To determine the V_{oc} of the current investigation a donor polymer (**J52-Cl**) is utilized. In Table 7, the calculated values of V_{oc} are illustrated along with the E_{LUMO} of **D1**, **D2**, **D3**, **D5** and **D7** in relation to the E_{HOMO} of the donor polymer (**J52-Cl**).

$$\Delta E = E_{LUMO}^A - E_{HOMO}^D$$

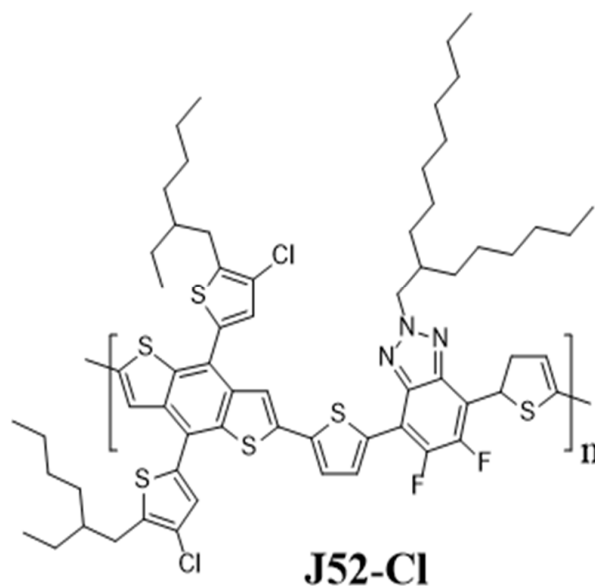


Figure 7. The structural representation of chlorinated polymer **J52-Cl**.

Table 7. Computed V_{oc} of **D1**, **D2**, **D3**, **D5** and **D7**.

Chromophores	V_{oc} (V)	ΔE
D1	1.549	1.849
D2	1.584	1.884
D3	1.600	1.900
D5	1.624	1.924
D7	1.632	1.932

The V_{oc} value for **D1**, **D2**, **D3**, **D5** and **D7** with respect to $LUMO_{acceptor}$ – $HOMO_{donor}$ energy difference is determined to be 1.549, 1.584, 1.600, 1.624 and 1.632 V, respectively. The V_{oc} of entitled compounds decreases in the following order: **D7** > **D5** > **D3** > **D2** > **D1**. Among all tailored molecules, **D7** displayed the highest V_{oc} (1.632 V). Since the transference of electrons from donor (D) to acceptor (A) segments, the HOMO/LUMO energy gap is a crucial tool for improving the PCEs of solar cells. A low-lying LUMO lead to improved V_{oc} values having better optoelectronic properties. Open-circuit voltage (V_{oc}) diagram is illustrated in Figure 8. This form of molecular orbital alignment makes it easier for the electron density to move from the donor polymer to the acceptor, as all our derivatives possess a lower value of LUMO than the **J52Cl**, which improves optoelectronic behavior.

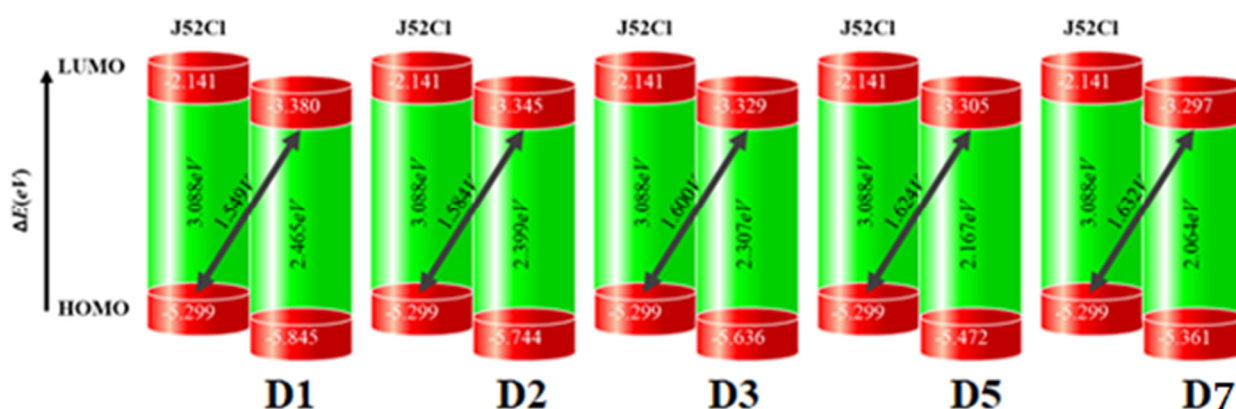


Figure 8. The V_{oc} diagram of **D1**, **D2**, **D3**, **D5** and **D7** with respect to donor **JCl52**.

6. Conclusions

The organic-based materials (**D1**, **D2**, **D3**, **D5** and **D7**) have been designed through the incorporation of selenophene units in the reference compound (**DF-PCIC**) up to $n = 7$. In order to improve the electron-withdrawing effect of terminal acceptors, benzothiophene-based acceptors are also introduced in **D1**, **D2**, **D3**, **D5** and **D7** compounds. After the addition of selenophene units, diminishing in band gaps ($\Delta E = 2.399 - 2.064$ eV) accompanied by larger bathochromic shift ($\lambda_{max} = 655.480 - 728.376$ nm) and lower binding energies ($E_b = 0.508 - 0.362$ eV) are obtained, and the conjugation is also enhanced. These findings enclosed higher exciton dissociation rate and significant charge transference from HOMO to LUMO, which is further supported by TDM and DOS analyses. The GRP studies and diminishing band gaps revealed that increasing conjugation grants significant stability to the computed chromophores. An efficient value of V_{oc} is noticed for all POSCs materials when determined with respect to **JCl52** polymer. Among all the compounds, **D7** exhibited a lower bandgap (2.064 eV) and highest λ_{max} (691.953 nm in gas and 728.376 nm in chloroform) and greater open-circuit voltage value (1.632 V), which proves that it is a most suitable chromophore with outstanding photovoltaic characteristics. Consequently, significant photovoltaic materials can be developed by structural tailoring with selenophene units and efficient electron-withdrawing moieties. Moreover, this study also encourages the experimentalist to synthesize these efficient materials.

Supplementary Materials: The following are available online at <https://www.mdpi.com/article/10.3390/polym15061508/s1>. It contain cartesian co-ordinates, molecular orbital energies, UV-Vis absorption values, FMOs diagrams showed movement of charges transference between orbitals and ICUPAC names of studied selenophene based compounds.

Author Contributions: M.N.A.: Data curation; formal analysis; writing draft. I.S.: Conceptualization; methodology, writing. M.K.: Methodology; software; writing and editing draft. M.A.: Conceptualization; methodology; software. A.M.A.: Conceptualization; resources. M.M.A.: Data curation; formal analysis; validation. A.A.C.B.; methodology; software. A.K.; Conceptualization;

K.A.A. Writing-review & editing. All authors have read and agreed to the published version of the manuscript.

Funding: Institutional Fund Projects under grant no (IFPRC-102-130-2020).

Institutional Review Board Statement: Not applicable.

Informed Consent Statement: Not applicable.

Data Availability Statement: All data generated or analyzed during this study are included in this published article and its Supplementary Information Files.

Acknowledgments: This research work was funded by Institutional Fund Projects under grant no (IFPRC-102-130-2020). Therefore, authors gratefully acknowledge technical and financial support from the Ministry of Education and King Abdulaziz University, Jeddah, Saudi Arabia.

Conflicts of Interest: There is no conflict of interest of any type to influence the work reported in this paper.

References

1. Cheng, P.; Li, G.; Zhan, X.; Yang, Y. Next-generation organic photovoltaics based on non-fullerene acceptors. *Nat. Photonics* **2018**, *12*, 131–142. [\[CrossRef\]](#)
2. Yan, C.; Barlow, S.; Wang, Z.; Yan, H.; Jen, A.K.-Y.; Marder, S.R.; Zhan, X. Non-fullerene acceptors for organic solar cells. *Nat. Rev. Mater.* **2018**, *3*, 18003. [\[CrossRef\]](#)
3. Ans, M.; Iqbal, J.; Ayub, K.; Ali, E.; Eliasson, B. Spirobifluorene based small molecules as an alternative to traditional fullerene acceptors for organic solar cells. *Mater. Sci. Semicond. Process.* **2019**, *94*, 97–106. [\[CrossRef\]](#)
4. Zhu, J.; Xiao, Y.; Wang, J.; Liu, K.; Jiang, H.; Lin, Y.; Lu, X.; Zhan, X. Alkoxy-induced near-infrared sensitive electron acceptor for high-performance organic solar cells. *Chem. Mater.* **2018**, *30*, 4150–4156. [\[CrossRef\]](#)
5. Aldrich, T.J.; Matta, M.; Zhu, W.; Swick, S.M.; Stern, C.L.; Schatz, G.C.; Facchetti, A.; Melkonyan, F.S.; Marks, T.J. Fluorination effects on indacenodithienothiophene acceptor packing and electronic structure, end-group redistribution, and solar cell photovoltaic response. *J. Am. Chem. Soc.* **2019**, *141*, 3274–3287. [\[CrossRef\]](#)
6. Qi, Q.; Guo, X.; Zhu, B.; Deng, P.; Zhan, H.; Yang, J. Side-chain optimization of perylene diimide-thiophene random terpolymer acceptors for enhancing the photovoltaic efficiency of all-polymer solar cells. *Org. Electron.* **2020**, *78*, 105616. [\[CrossRef\]](#)
7. Wang, H.; Li, M.; Liu, Y.; Song, J.; Li, C.; Bo, Z. Perylene diimide based star-shaped small molecular acceptors for high efficiency organic solar cells. *J. Mater. Chem. C* **2019**, *7*, 819–825. [\[CrossRef\]](#)
8. Meng, D.; Sun, D.; Zhong, C.; Liu, T.; Fan, B.; Huo, L.; Li, Y.; Jiang, W.; Choi, H.; Kim, T. High-performance solution-processed non-fullerene organic solar cells based on selenophene-containing perylene bisimide acceptor. *J. Am. Chem. Soc.* **2016**, *138*, 375–380. [\[CrossRef\]](#)
9. Mathew, S.; Yella, A.; Gao, P.; Humphry-Baker, R.; Curchod, B.F.; Ashari-Astani, N.; Tavernelli, I.; Rothlisberger, M.; Nazeeruddin, M. Grätzel, Dye-sensitized solar cells with 13% efficiency achieved through the molecular engineering of porphyrin sensitizers. *Nat. Chem.* **2014**, *6*, 242–247. [\[CrossRef\]](#)
10. Hagfeldt, A.; Boschloo, G.; Sun, L.; Kloo, L.; Pettersson, H. Dye-sensitized solar cells. *Chem. Rev.* **2010**, *110*, 6595–6663. [\[CrossRef\]](#)
11. Grätzel, M. Conversion of sunlight to electric power by nanocrystalline dye-sensitized solar cells. *J. Photochem. Photobiol. A Chem.* **2004**, *164*, 3–14. [\[CrossRef\]](#)
12. Mishra, A.; Fischer, M.K.; Bäuerle, P. Metal-free organic dyes for dye-sensitized solar cells: From structure: Property relationships to design rules. *Angew. Chem. Int. Ed.* **2009**, *48*, 2474–2499. [\[CrossRef\]](#)
13. Cheng, Y.-J.; Yang, S.-H.; Hsu, C.-S. Synthesis of conjugated polymers for organic solar cell applications. *Chem. Rev.* **2009**, *109*, 5868–5923. [\[CrossRef\]](#)
14. Lin, Y.; Li, Y.; Zhan, X. Small molecule semiconductors for high-efficiency organic photovoltaics. *Chem. Soc. Rev.* **2012**, *41*, 4245–4272. [\[CrossRef\]](#) [\[PubMed\]](#)
15. Wei, Y.; Chen, Z.; Lu, G.; Yu, N.; Li, C.; Gao, J.; Gu, X.; Hao, X.; Lu, G.; Tang, Z. Binary organic solar cells breaking 19% via manipulating the vertical component distribution. *Adv. Mater.* **2022**, *34*, 2204718. [\[CrossRef\]](#) [\[PubMed\]](#)
16. Hamblin, M.R. Fullerenes as photosensitizers in photodynamic therapy: Pros and cons. *Photochem. Photobiol. Sci.* **2018**, *17*, 1515–1533. [\[CrossRef\]](#)
17. Zhao, J.; Li, Y.; Yang, G.; Jiang, K.; Lin, H.; Ade, H.; Ma, W.; Yan, H. Efficient organic solar cells processed from hydrocarbon solvents. *Nat. Energy* **2016**, *1*, 15027. [\[CrossRef\]](#)
18. Ran, N.A.; Love, J.A.; Takacs, C.J.; Sadhanala, A.; Beavers, J.K.; Collins, S.D.; Huang, Y.; Wang, M.; Friend, R.H.; Bazan, G.C. Harvesting the full potential of photons with organic solar cells. *Adv. Mater.* **2016**, *28*, 1482–1488. [\[CrossRef\]](#)
19. Liu, J.; Chen, S.; Qian, D.; Gautam, B.; Yang, G.; Zhao, J.; Bergqvist, J.; Zhang, F.; Ma, W.; Ade, H. Fast charge separation in a non-fullerene organic solar cell with a small driving force. *Nat. Energy* **2016**, *1*, 16089. [\[CrossRef\]](#)
20. Li, Y. Molecular design of photovoltaic materials for polymer solar cells: Toward suitable electronic energy levels and broad absorption. *Acc. Chem. Res.* **2012**, *45*, 723–733. [\[CrossRef\]](#)

21. Chen, J.; Cao, Y. Development of novel conjugated donor polymers for high-efficiency bulk-heterojunction photovoltaic devices. *Acc. Chem. Res.* **2009**, *42*, 1709–1718. [[CrossRef](#)] [[PubMed](#)]
22. Wielopolski, M.; Kim, J.-H.; Jung, Y.-S.; Yu, Y.-J.; Kay, K.-Y.; Holcombe, T.W.; Zakeeruddin, S.M.; Grätzel, M.; Moser, J.-E. Position-dependent extension of π -conjugation in D- π -A dye sensitizers and the impact on the charge-transfer properties. *J. Phys. Chem. C* **2013**, *117*, 13805–13815. [[CrossRef](#)]
23. Khan, M.U.; Khalid, M.; Shafiq, I.; Khera, R.A.; Shafiq, Z.; Jawaria, R.; Shafiq, M.; Alam, M.M.; Braga, A.A.C.; Imran, M. Theoretical investigation of nonlinear optical behavior for rod and T-Shaped phenothiazine based D- π -A organic compounds and their derivatives. *J. Saudi Chem. Soc.* **2021**, *25*, 101339. [[CrossRef](#)]
24. Yan, T.; Song, W.; Huang, J.; Peng, R.; Huang, L.; Ge, Z. 16.67% rigid and 14.06% flexible organic solar cells enabled by ternary heterojunction strategy. *Adv. Mater.* **2019**, *31*, 1902210. [[CrossRef](#)]
25. Yuan, J.; Zhang, Y.; Zhou, L.; Zhang, G.; Yip, H.-L.; Lau, T.-K.; Lu, X.; Zhu, C.; Peng, H.; Johnson, P.A. Single-junction organic solar cell with over 15% efficiency using fused-ring acceptor with electron-deficient core. *Joule* **2019**, *3*, 1140–1151. [[CrossRef](#)]
26. Fan, B.; Du, X.; Liu, F.; Zhong, W.; Ying, L.; Xie, R.; Tang, X.; An, K.; Xin, J.; Li, N. Fine-tuning of the chemical structure of photoactive materials for highly efficient organic photovoltaics. *Nat. Energy* **2018**, *3*, 1051–1058. [[CrossRef](#)]
27. Clarke, T.M.; Durrant, J.R. Charge photogeneration in organic solar cells. *Chem. Rev.* **2010**, *110*, 6736–6767. [[CrossRef](#)]
28. Che, X.; Li, Y.; Qu, Y.; Forrest, S.R. High fabrication yield organic tandem photovoltaics combining vacuum-and solution-processed subcells with 15% efficiency. *Nat. Energy* **2018**, *3*, 422–427. [[CrossRef](#)]
29. Qin, J.; Zhang, L.; Zuo, C.; Xiao, Z.; Yuan, Y.; Yang, S.; Hao, F.; Cheng, M.; Sun, K.; Bao, Q. A chlorinated copolymer donor demonstrates a 18.13% power conversion efficiency. *J. Semicond.* **2021**, *42*, 010501. [[CrossRef](#)]
30. Peters, C.H.; Sachs-Quintana, I.T.; Kastrop, J.P.; Beaupre, S.; Leclerc, M.; McGehee, M.D. High efficiency polymer solar cells with long operating lifetimes. *Adv. Energy Mater.* **2011**, *1*, 491–494. [[CrossRef](#)]
31. Jørgensen, M.; Norrman, K.; Gevorgyan, S.A.; Tromholt, T.; Andreasen, B.; Krebs, F.C. Stability of polymer solar cells. *Adv. Mater.* **2012**, *24*, 580–612. [[CrossRef](#)] [[PubMed](#)]
32. Liu, Z.; Zeng, D.; Gao, X.; Li, P.; Zhang, Q.; Peng, X. Non-fullerene polymer acceptors based on perylene diimides in all-polymer solar cells. *Sol. Energy Mater. Sol. Cells* **2019**, *189*, 103–117. [[CrossRef](#)]
33. Li, S.; Ye, L.; Zhao, W.; Yan, H.; Yang, B.; Liu, D.; Li, W.; Ade, H.; Hou, J. A wide band gap polymer with a deep highest occupied molecular orbital level enables 14.2% efficiency in polymer solar cells. *J. Am. Chem. Soc.* **2018**, *140*, 7159–7167. [[CrossRef](#)] [[PubMed](#)]
34. Li, S.; Ye, L.; Zhao, W.; Zhang, S.; Mukherjee, S.; Ade, H.; Hou, J. Energy-level modulation of small-molecule electron acceptors to achieve over 12% efficiency in polymer solar cells. *Adv. Mater.* **2016**, *28*, 9423–9429. [[CrossRef](#)]
35. Zhao, F.; Dai, S.; Wu, Y.; Zhang, Q.; Wang, J.; Jiang, L.; Ling, Q.; Wei, Z.; Ma, W.; You, W. Single-junction binary-blend nonfullerene polymer solar cells with 12.1% efficiency. *Adv. Mater.* **2017**, *29*, 1700144. [[CrossRef](#)]
36. Li, Z.; Jiang, K.; Yang, G.; Lai, J.Y.L.; Ma, T.; Zhao, J.; Ma, W.; Yan, H. Donor polymer design enables efficient non-fullerene organic solar cells. *Nat. Commun.* **2016**, *7*, 13094. [[CrossRef](#)]
37. Khalid, A.; Khera, R.A.; Saeed, A.; Khalid, M.; Iqbal, S.; Iqbal, J. Designing benzothiadiazole based non-fullerene acceptors with high open circuit voltage and higher LUMO level to increase the efficiency of organic solar cells. *Optik* **2021**, *228*, 166138. [[CrossRef](#)]
38. Kroon, R.; Lenes, M.; Hummelen, J.C.; Blom, P.W.; De Boer, B. Small bandgap polymers for organic solar cells (polymer material development in the last 5 years). *Polym. Rev.* **2008**, *48*, 531–582. [[CrossRef](#)]
39. Roncali, J. Synthetic principles for bandgap control in linear π -conjugated systems. *Chem. Rev.* **1997**, *97*, 173–206. [[CrossRef](#)]
40. Fichou, D.; Watanabe, T.; Takeda, T.; Miyata, S.; Goto, Y.; Nakayama, M. Influence of the ring-substitution on the second harmonic generation of chalcone derivatives. *Jpn. J. Appl. Phys.* **1988**, *27*, L4291988. [[CrossRef](#)]
41. Li, S.; Zhan, L.; Liu, F.; Ren, J.; Shi, M.; Li, C.-Z.; Russell, T.P.; Chen, H. An unfused-core-based nonfullerene acceptor enables high-efficiency organic solar cells with excellent morphological stability at high temperatures. *Adv. Mater.* **2018**, *30*, 1705208. [[CrossRef](#)]
42. Khalid, M.; Ahmed, R.; Arshad, M.; Asghar, M.A.; Munawar, K.S.; Imran, M.; Braga, A.A. First theoretical framework for highly efficient photovoltaic parameters by structural modification with benzothiophene-incorporated acceptors in dithiophene based chromophores. *Sci. Rep.* **2022**, *12*, 20148. [[CrossRef](#)]
43. Kim, B.; Yeom, H.R.; Yun, M.H.; Kim, J.Y.; Yang, C. A selenophene analogue of PCDTBT: Selective fine-tuning of lumo to lower of the bandgap for efficient polymer solar cells. *Macromolecules* **2012**, *45*, 8658–8664. [[CrossRef](#)]
44. Kranthiraja, K.; Gunasekar, K.; Cho, W.; Park, Y.G.; Lee, J.Y.; Shin, Y.; Kang, I.-N.; Song, M.; Chae, K.H.; Kim, B. Influential effects of π -spacers, alkyl side chains, and various processing conditions on the photovoltaic properties of alkylselenyl substituted benzodithiophene based polymers. *J. Mater. Chem. C* **2015**, *3*, 796–808. [[CrossRef](#)]
45. Chang, S.-L.; Hung, K.-E.; Cao, F.-Y.; Huang, K.-H.; Hsu, C.-S.; Liao, C.-Y.; Lee, C.-H.; Cheng, Y.-J. Isomerically Pure Benzothiophene-Incorporated Acceptor: Achieving Improved V_{OC} and J_{SC} of Nonfullerene Organic Solar Cells via End Group Manipulation. *ACS Appl. Mater. Interfaces* **2019**, *11*, 33179–33187. [[CrossRef](#)]
46. Frisch, M.; Trucks, G.W.; Schlegel, H.B.; Scuseria, G.E.; Robb, M.A.; Cheeseman, J.R.; Scalmani, G.; Barone, V.; Mennucci, B.; Petersson, G.A. Gaussian 09, revision D. 01. 2009. Available online: <https://gaussian.com/g09citation> (accessed on 17 February 2023).

47. Dennington, R.D.; Keith, T.A.; Millam, J.M. *GaussView 5.0*; Gaussian, Inc.: Wallingford, UK, 2008; p. 20.
48. Hanwell, M.D.; Curtis, D.E.; Lonie, D.C.; Vandermeersch, T.; Zurek, E.; Hutchison, G.R. Avogadro: An advanced semantic chemical editor, visualization, and analysis platform. *J. Cheminform.* **2012**, *4*, 17. [CrossRef]
49. O'boyle, N.M.; Tenderholt, A.L.; Langner, K.M. Cclib: A library for package-independent computational chemistry algorithms. *J. Comput. Chem.* **2008**, *29*, 839–845. [CrossRef] [PubMed]
50. Zhurko, G.A. Chemcraft. Available online: <http://www.chemcraftprog.com> (accessed on 22 October 2022).
51. Lu, T.; Chen, F. Multiwfn: A multifunctional wavefunction analyzer. *J. Comput. Chem.* **2012**, *33*, 580–592. [CrossRef] [PubMed]
52. Cclib: A library for Package-Independent Computational Chemistry Algorithms—O'boyle—2008—Journal of Computational Chemistry—Wiley Online Library, (n.d.). Available online: <https://onlinelibrary.wiley.com/doi/10.1002/jcc.20823> (accessed on 26 October 2022).
53. Stevenson, K.J. Review of originpro 8.5. *J. Am. Chem. Soc.* **2011**, *133*, 5621. [CrossRef]
54. Li, G.; Budiawan, W.; Wang, P.C.; Chu, C.W. Conjugated Polymer-Based Solar Cells. In *Encyclopedia of Modern Optics*; Elsevier: Amsterdam, The Netherlands, 2018; pp. 256–269. [CrossRef]
55. Kesavan, A.V.; Ramamurthy, P.C. Photo-Active Polymer Nanocomposite Layer for Energy Applications. In *Polymer-Based Advanced Functional Composites for Optoelectronic and Energy Applications*; Elsevier: Amsterdam, The Netherlands, 2021; pp. 135–156. [CrossRef]
56. Kulhánek, J.; Bureš, F. Imidazole as a parent π -conjugated backbone in charge-transfer chromophores. *Beilstein J. Org. Chem.* **2012**, *8*, 25–49. [CrossRef] [PubMed]
57. Patra, A.; Wijsboom, Y.H.; Leitus, G.; Bendikov, M. Tuning the band gap of low-band-gap polyselenophenes and polythiophenes: The effect of the heteroatom. *Chem. Mater.* **2011**, *23*, 896–906. [CrossRef]
58. Asogwa, F.C.; Louis, H.; Ameuru, U.S.; Unimuke, T.O.; Adekoge, K.A.; Magu, T.O.; Agwamba, E.C. Experimental and theoretical studies of the influence of alkyl groups on the photovoltaic properties of (E)-6-((2, 3-dihydroxynaphthalene) diazenyl)-1H-benzoisoquinoline-1, 3-dione-based organic solar cell. *J. Mol. Model.* **2022**, *28*, 1–18. [CrossRef]
59. Srnec, M.; Solomon, E.I. Frontier molecular orbital contributions to chlorination versus hydroxylation selectivity in the non-heme iron halogenase SyrB2. *J. Am. Chem. Soc.* **2017**, *139*, 2396–2407. [CrossRef] [PubMed]
60. Khan, M.U.; Iqbal, J.; Khalid, M.; Hussain, R.; Braga, A.A.C.; Hussain, M.; Muhammad, S. Designing triazatruxene-based donor materials with promising photovoltaic parameters for organic solar cells. *RSC Adv.* **2019**, *9*, 26402–26418. [CrossRef] [PubMed]
61. Khalid, M.; Khan, M.U.; Shafiq, I.; Hussain, R.; Ali, A.; Imran, M.; Braga, A.A.; Rehman, M.F.U.; Akram, M.S. Structural modulation of π -conjugated linkers in D- π -A dyes based on triphenylamine dicyanovinylene framework to explore the NLO properties. *R. Soc. Open Sci.* **2021**, *8*, 210570. [CrossRef]
62. Kandemirli, F.; Sagdinc, S. Theoretical study of corrosion inhibition of amides and thiosemicarbazones. *Corros. Sci.* **2007**, *49*, 2118–2130. [CrossRef]
63. Mahmood, A.; Abdullah, M.I.; Khan, S.U.-D. Enhancement of nonlinear optical (NLO) properties of indigo through modification of auxiliary donor, donor and acceptor. *Spectrochim. Acta Part A Mol. Biomol. Spectrosc.* **2015**, *139*, 425–430. [CrossRef]
64. Mahmood, A.; Khan, S.U.-D.; Rana, U.A.; Janjua, M.R.S.A.; Tahir, M.H.; Nazar, M.F.; Song, Y. Effect of thiophene rings on UV/visible spectra and non-linear optical (NLO) properties of triphenylamine based dyes: A quantum chemical perspective. *J. Phys. Org. Chem.* **2015**, *28*, 418–422. [CrossRef]
65. Khalid, M.; Imran, M.; Braga, A.A.C.; Akram, M.S. Molecular engineering of indenoindene-3-ethylrodanine acceptors with A2-A1-D-A1-A2 architecture for promising fullerene-free organic solar cells. *Sci. Rep.* **2021**, *11*, 20320. [CrossRef]
66. Hussain, S.; Hussain, R.; Mehboob, M.Y.; Chatha, S.A.S.; Hussain, A.I.; Umar, A.; Khan, M.U.; Ahmed, M.; Adnan, M.; Ayub, K. Adsorption of phosgene gas on pristine and copper-decorated B12N12 nanocages: A comparative DFT study. *ACS Omega* **2020**, *5*, 7641–7650. [CrossRef]
67. Hussain, S.; Chatha, S.A.S.; Hussain, A.I.; Hussain, R.; Mehboob, M.Y.; Muhammad, S.; Ahmad, Z.; Ayub, K. Zinc-doped boron phosphide nanocluster as efficient sensor for SO₂. *J. Chem.* **2020**, *2020*, 2629596. [CrossRef]
68. Mahmood, A.; Hussain Tahir, M.; Irfan, A.; Khalid, B.; Al-Sehemi, A.G. Computational designing of triphenylamine dyes with broad and red-shifted absorption spectra for dye-sensitized solar cells using multi-thiophene rings in π -spacer. *Bull. Korean Chem. Soc.* **2015**, *36*, 2615–2620. [CrossRef]
69. Khalid, M. First principles study of electronic and nonlinear optical properties of A-D- π -A and D-A-D- π -A configured compounds containing novel quinoline-carbazole derivatives. *RSC Adv.* **2020**, *10*, 22273–22283. [CrossRef]
70. Parr, R.G.; Szentpály, L.V.; Liu, S. Electrophilicity index. *J. Am. Chem. Soc.* **1999**, *121*, 1922–1924. [CrossRef]
71. Fukui, K. Role of frontier orbitals in chemical reactions. *Science* **1982**, *218*, 747–754. [CrossRef] [PubMed]
72. Chattaraj, P.K. Electrophilicity Index. *Chem. Rev.* **2011**, *111*, PR43–PR75. [CrossRef]
73. Parr, R.G.; Donnelly, R.A.; Levy, M.; Palke, W.E. Electronegativity: The density functional viewpoint. *J. Chem. Phys.* **1978**, *68*, 3801–3807. [CrossRef]
74. Kovačević, N.; Kokalj, A. Analysis of molecular electronic structure of imidazole-and benzimidazole-based inhibitors: A simple recipe for qualitative estimation of chemical hardness. *Corros. Sci.* **2011**, *53*, 909–921. [CrossRef]
75. Koopmans, T. Über die Zuordnung von Wellenfunktionen und Eigenwerten zu den einzelnen Elektronen eines Atoms. *Physica* **1934**, *1*, 104–113. [CrossRef]

76. He, S.; Tan, Y.; Xiao, X.; Zhu, L.; Guo, Y.; Li, M.; Tian, A.; Pu, X.; Wong, N.-B. Substituent effects on electronic character of the CN group and trans/cis isomerization in the C-substituted imine derivatives: A computational study. *J. Mol. Struct. Theochem.* **2010**, *951*, 7–13. [[CrossRef](#)]
77. Tahir, M.N.; Khalid, M.; Islam, A.; Mashhadi, S.M.A.; Braga, A.A. Facile synthesis, single crystal analysis, and computational studies of sulfanilamide derivatives. *J. Mol. Struct.* **2017**, *1127*, 766–776. [[CrossRef](#)]
78. Khalid, M.; Lodhi, H.M.; Khan, M.U.; Imran, M. Structural parameter-modulated nonlinear optical amplitude of acceptor- π -D- π -donor-configured pyrene derivatives: A DFT approach. *RSC Adv.* **2021**, *11*, 14237–14250. [[CrossRef](#)]
79. Shehzad, R.A.; Iqbal, J.; Khan, M.U.; Hussain, R.; Javed, H.M.A.; Rehman, A.U.; Alvi, M.U.; Khalid, M. Designing of benzothiazole based non-fullerene acceptor (NFA) molecules for highly efficient organic solar cells. *Comput. Theor. Chem.* **2020**, *1181*, 112833. [[CrossRef](#)]
80. Khan, M.U.; Mehboob, M.Y.; Hussain, R.; Afzal, Z.; Khalid, M.; Adnan, M. Designing spirobifullerene core based three-dimensional cross shape acceptor materials with promising photovoltaic properties for high-efficiency organic solar cells. *Int. J. Quantum Chem.* **2020**, *120*, e263772020. [[CrossRef](#)]
81. Ans, M.; Ayub, K.; Bhatti, I.A.; Iqbal, J. Designing indacenodithiophene based non-fullerene acceptors with a donor-acceptor combined bridge for organic solar cells. *RSC Adv.* **2019**, *9*, 3605–3617. [[CrossRef](#)] [[PubMed](#)]
82. Mahmood, A.; Irfan, A.; Ahmad, F.; Janjua, M.R.S.A. Quantum chemical analysis and molecular dynamics simulations to study the impact of electron-deficient substituents on electronic behavior of small molecule acceptors. *Comput. Theor. Chem.* **2021**, *1204*, 113387. [[CrossRef](#)]
83. Li, Y.; Ullrich, C.A. Time-dependent transition density matrix. *Chem. Phys.* **2011**, *391*, 157–163. [[CrossRef](#)]
84. Khalid, M.; Khan, M.; Shafiq, I.; Mahmood, K.; Akhtar, M.N.; Iqbal, J.; Al-Sadoon, M.K.; Zaman, W.; Braga, A.A.C. Role of donors in triggering second order non-linear optical properties of non-fullerene FCO-2FR1 based derivatives: A theoretical perspective. *Heliyon* **2023**, *9*, e130332023. [[CrossRef](#)]
85. Arshad, M.N.; Shafiq, I.; Khalid, M.; Asiri, A.M. Exploration of the Intriguing Photovoltaic Behavior for Fused Indacenodithiophene-Based A-D-A Conjugated Systems: A DFT Model Study. *ACS Omega* **2022**, *7*, 11606–11617. [[CrossRef](#)]
86. Hussain, R.; Hassan, F.; Khan, M.U.; Mehboob, M.Y.; Fatima, R.; Khalid, M.; Mahmood, K.; Tariq, C.J.; Akhtar, M.N. Molecular engineering of A-D-C-D-A configured small molecular acceptors (SMAs) with promising photovoltaic properties for high-efficiency fullerene-free organic solar cells. *Opt. Quantum Electron.* **2020**, *52*, 364. [[CrossRef](#)]
87. Khan, M.U.; Mehboob, M.Y.; Hussain, R.; Fatima, R.; Tahir, M.S.; Khalid, M.; Braga, A.A.C. Molecular designing of high-performance 3D star-shaped electron acceptors containing a truxene core for nonfullerene organic solar cells. *J. Phys. Org. Chem.* **2021**, *34*, e4119. [[CrossRef](#)]
88. Irfan, M.; Iqbal, J.; Sadaf, S.; Eliasson, B.; Rana, U.A.; Khan, S.U.-D.; Ayub, K. Design of donor-acceptor-donor (D-A-D) type small molecule donor materials with efficient photovoltaic parameters: IRFAN et al. *Int. J. Quantum Chem.* **2017**, *117*, e253632017. [[CrossRef](#)]
89. Khalid, M.; Shafiq, I.; Zhu, M.; Khan, M.U.; Shafiq, Z.; Iqbal, J.; Alam, M.M.; Braga, A.A.C.; Imran, M. Efficient tuning of small acceptor chromophores with A1- π -A2- π -A1 configuration for high efficacy of organic solar cells via end group manipulation. *J. Saudi Chem. Soc.* **2021**, *25*, 101305. [[CrossRef](#)]
90. Mahmood, A. Photovoltaic and charge transport behavior of diketopyrrolopyrrole based compounds with A-D-A-D-A skeleton. *J. Clust. Sci.* **2019**, *30*, 1123–1130. [[CrossRef](#)]
91. Bai, H.; Wang, Y.; Cheng, P.; Li, Y.; Zhu, D.; Zhan, X. Acceptor-Donor-Acceptor Small Molecules Based on Indacenodithiophene for Efficient Organic Solar Cells. *ACS Appl. Mater. Interfaces* **2014**, *6*, 8426–8433. [[CrossRef](#)] [[PubMed](#)]
92. Scharber, M.C.; Mühlbacher, D.; Koppe, M.; Denk, P.; Waldauf, C.; Heeger, A.J.; Brabec, C.J. Design Rules for Donors in Bulk-Heterojunction Solar Cells—Towards 10% Energy-Conversion Efficiency. *Adv. Mater.* **2006**, *18*, 789–794. [[CrossRef](#)]
93. Khalid, M.; Khan, M.U.; Razia, E.; Shafiq, Z.; Alam, M.M.; Imran, M.; Akram, M.S. Exploration of efficient electron acceptors for organic solar cells: Rational design of indacenodithiophene based non-fullerene compounds. *Sci. Rep.* **2021**, *11*, 19931. [[CrossRef](#)] [[PubMed](#)]
94. Li, J.; Li, F.; Zhang, B.; Zhou, E. Synthesis of 1-formyl-3-bromo-thieno [3, 4-c] pyrrole-4, 6-dione and the application in A2-A1-D-A1-A2 type non-fullerene acceptor. *J. Phys. Chem. C* **2020**, *124*, 9795–9801. [[CrossRef](#)]
95. Tang, A.; Zhang, Q.; Du, M.; Li, G.; Geng, Y.; Zhang, J.; Wei, Z.; Sun, X.; Zhou, E. Molecular engineering of D- π -A copolymers based on 4, 8-bis (4-chlorothiophen-2-yl) benzo [1, 2-b: 4, 5-b'] dithiophene (BDT-T-Cl) for high-performance fullerene-free organic solar cells. *Macromolecules* **2019**, *52*, 6227–6233. [[CrossRef](#)]
96. Tang, A.; Song, W.; Xiao, B.; Guo, J.; Min, J.; Ge, Z.; Zhang, J.; Wei, Z.; Zhou, E. Benzotriazole-based acceptor and donors, coupled with chlorination, achieve a high V OC of 1.24 V and an efficiency of 10.5% in fullerene-free organic solar cells. *Chem. Mater.* **2019**, *31*, 3941–3947. [[CrossRef](#)]

Disclaimer/Publisher's Note: The statements, opinions and data contained in all publications are solely those of the individual author(s) and contributor(s) and not of MDPI and/or the editor(s). MDPI and/or the editor(s) disclaim responsibility for any injury to people or property resulting from any ideas, methods, instructions or products referred to in the content.